Inorg. Chem. **2006**, *45*, 201–213

Facilitating Access to the Most Easily Ionized Molecule: an Improved Synthesis of the Key Intermediate, $W_2(hpp)_4Cl_2$, and Related Compounds

F. Albert Cotton,*,† James P. Donahue,†,‡ Nadine E. Gruhn,£ Dennis L. Lichtenberger,*,£ Carlos A. Murillo,*,† Daren J. Timmons,†,§ Laura O. Van Dorn,£ Dino Villagrán,† and Xiaoping Wang†

Department of Chemistry, Laboratory for Molecular Structure and Bonding, P.O. Box 30012, Texas A&M University, College Station, Texas 77842-3012, Department of Chemistry, Tulane University, New Orleans, Louisiana 70118, Department of Chemistry, Virginia Military Institute, Lexington, Virginia 24450-0304, and Department of Chemistry, Center for Gas-Phase Electron Spectroscopy, The University of Arizona, Tucson, Arizona 85721

Received September 13, 2005

A far superior synthesis is reported for $W_2(hpp)_4Cl_2$, a key intermediate in the synthesis of the most easily ionized closed-shell molecule $W_2(hpp)_4$ (hpp = the anion of the bicyclic guanidine compound 1,3,4,6,7,8-hexahydro-2*H*-pyrimido[1,2-*a*]pyrimidine). At 200 °C, the one-pot reaction of the air-stable and commercially available compounds $W(CO)_6$ and Hhpp in *o*-dichlorobenzene produces $W_2(hpp)_4Cl_2$ in multigram quantities with isolated yields of over 90%. At lower temperatures, the reaction can lead to other compounds such as $W(Hhpp)_2(CO)_4$ or $W_2(\mu\text{-}CO)_2(\mu\text{-}hpp)_2(\eta^2\text{-}hpp)_2$, which are isolable in good purity depending upon the specific conditions employed. These compounds provide insight into the reaction pathway to $W_2(hpp)_4Cl_2$ and $W_2(hpp)_4$. Two additional derivatives, $W_2(hpp)_4X_2$ where X is PF_6^- or the anion tetrakis[3,5-bis(trifluoromethyl)phenyl]borate (TFPB), have also been synthesized and structurally characterized. A comparison of the electrode potentials of $W_2(\mu\text{-}CO)_2(\mu\text{-}hpp)_2(\eta^2\text{-}hpp)_2$ and the di-*p*-anisylformamidinate analogue shows that oxidation of the hpp compound is significantly displaced (1.12 V) and shows that the bicyclic guanidinate ligand is considerably better than the formamidinate anion at stabilizing high oxidation states. A differential pulse voltammogram of $W_2(hpp)_4(TFPB)_2$ in THF shows two reduction processes with an $E_{1/2}$ of –0.97 V for the first and –1.81 V (vs Ag/AgCl) for the second. DFT calculations on the $W_2(hpp)_4^{2+}$ units in $W_2(hpp)_4X_2$ compounds show that the metal–metal bonding orbitals are destabilized by the axial ligands, which accounts for significant variations in the W–W distances. The low-energy gas-phase ionizations of $W_2(hpp)_4$ are also reported and discussed.

Introduction

Several years ago, we reported that the molecule $W_2(hpp)_4$ (hpp = 1,3,4,6,7,8-hexahydro-2*H*-pyrimido[1,2-*a*]pyrimidinate, Scheme 1) has an onset ionization energy of only 3.51 eV, making it the most easily ionized stable molecule known.[1] It even betters the cesium atom, commonly cited as the most easily oxidized of all neutral chemical entities,[2] by more than 0.35 eV. Despite the fact that it has a closed-shell electronic structure, it is more easily ionized than such famously strong reducing agents as $(\eta^6\text{-}C_6Me_6)(\eta^5\text{-}C_5Me_5)\text{-}Fe$[3] and $(\eta^5\text{-}C_5Me_5)_2Co$,[4] which have a lone electron sitting outside of their closed shells and ionization energies of 3.95 (onset) and 4.71 eV (vertical), respectively.[1] A theoretical

* To whom correspondence should be addressed. E-mail: cotton@tamu.edu (F.A.C.); dlichten@email.arizona.edu (D.L.L.); murillo@tamu.edu (C.A.M.).
† Texas A&M University.
‡ Tulane University.
§ Virginia Military Institute.
£ The University of Arizona.

(1) Cotton, F. A.; Gruhn, N. E.; Gu, J.; Huang, P.; Lichtenberger, D. L.; Murillo, C. A.; Van Dorn, L. O.; Wilkinson, C. C. *Science* **2002**, *298*, 1971.
(2) (a) Moore, C. E. *NSRDS-NBS 34*; National Bureau of Standards, Washington, DC, 1970. (b) Martin, W. C.; Wiese, W. L. In *Atomic, Molecular & Optical Physics Handbook*; F. Drake, G. W. F., Ed.; AIP Press: Woodbury, NY, 1996.
(3) Green, J. C.; Kelly, M. R.; Payne, M. P.; Seddon, E. A.; Astruc, D.; Hamon, J.-R.; Michaud, P. *Organometallics* **1983**, *2*, 211.
(4) Cauletti, C.; Green, J. C.; Kelly, M. R.; Powell, P.; Van Tilborg, J.; Robbins, J.; Smart, J. *J. Electron. Spectrosc. Relat. Phenom.* **1980**, *19*, 327.

10.1021/ic0515709 CCC: $33.50
Published on Web 12/07/2005

Scheme 1 . Structure of $W_2(hpp)_4$ and of the Molecules from Which the hpp and DAniF Ligands Are Derived

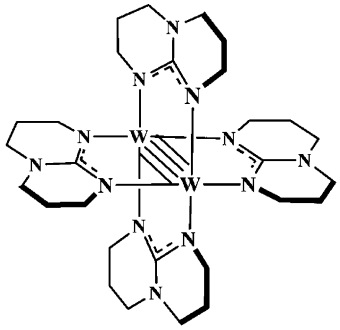

$W_2(hpp)_4$

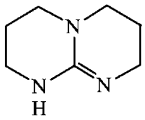

Hhpp = 1,3,4,6,7,8-hexahydro-2*H*-pyrimido[1,2-*a*]pyrimidine

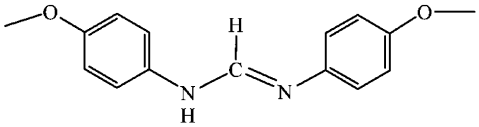

HDAniF = *N*,*N*′-di-*p*-anisylformamidine

explanation was also given in the previous report[1] to account for the easy ionization of $W_2(hpp)_4$, which is characterized by a strong interaction of the hpp pπ orbitals with the δ orbitals of the quadruply bonded W_2^{4+} unit.

Since the original report,[1] we have been concerned with making two important improvements in our understanding of the $W_2(hpp)_4$ molecule. One of these was to obtain a more complete and less noisy photoelectron spectrum (PES) for it; the other was to devise a superior method to prepare $W_2(hpp)_4$. Both of these goals have now been achieved.

The goal of having an efficient preparation of $W_2(hpp)_4$ is equivalent to having an efficient preparation of $W_2(hpp)_4Cl_2$ because reduction of $W_2(hpp)_4Cl_2$ by either $NaHBEt_3$[5] or potassium metal[6] with tetrahydrofuran as a solvent is very convenient and affords $W_2(hpp)_4$ in high yield. The intermediate $W_2(hpp)_4Cl_2$ is a very desirable species to work from since it is very stable, easily handled, and readily stockpiled for future use.

The method that we previously used[7] to prepare $W_2(hpp)_4Cl_2$, shown in the upper part of Scheme 2, required a sequence of reactions (for each of which the usual yield is given in bold in parentheses).

A route beginning with WCl_6 and $W(CO)_6$ and passing through (unisolated) $W_2Cl_8^{4-}$ has been used in the past for the syntheses of W_2^{4+} compounds.[8−12] A similar route for W_2^{6+} species using the same starting materials is rather lengthy and laborious.[7] An alternative multistep route, which was proposed later (see lower part of Scheme 2), requires the preparation and manipulation of many reactive intermediates.[13] Additionally, when the processes are considered from the starting reaction of $W(CO)_6$ with WCl_6 (which in itself requires purification by sublimation), the yields by the two pathways are essentially the same and are only 31−32%.

It is clear that the current methods of preparation of $W_2(hpp)_4$ would discourage most synthetic chemists from using it as a reducing agent. In the design of a more convenient method of preparation using relatively inexpensive and easily handled starting materials, the use of $W(CO)_6$ as the sole source of tungsten atoms came under consideration in view of the fact that it had previously been used to make quadruply bonded ditungsten compounds, notably with 2-hydroxy-6-methylpyridine,[14] 2-hydroxy-6-chloropyridine,[15] 2,4-dimethyl-6-hydroxypyrimidine,[16] and tetraphenylporphyrin.[17] These reactions share the common feature of requiring vigorous reflux (180−200 °C) in a high-boiling solvent such as diglyme or decalin. However, recent results had shown that the high-temperature reaction of $W(CO)_6$ with *N*,*N*′-di-*p*-anisylformamidine (HDAniF in Scheme 1)[18] was unable to expel all the carbonyl groups from $W(CO)_6$ and thus did not form the desired quadruply bonded, tetragonal paddlewheel complexes. This study revealed that, in addition to some edge-sharing bioctahedral compounds that had intact formamidinate ligands,[18] there were some complexes in which the HDAniF ligand is cleaved, indicating that the formamidinate ligand is susceptible to decomposition under the harsh conditions needed to provoke complete elimination of the carbonyl groups. Nevertheless, because we had previously noted that hpp is a considerably more robust ligand[19] that is also capable of stabilizing oxidation states in dimetal complexes[20] not accessible with the formamidinates, it was decided that it was worthwhile to proceed with a study of the reaction of $W(CO)_6$ with Hhpp. It was anticipated that such a reaction might produce, at least initially, partial substitution products, as has often been the

(5) Cotton, F. A.; Huang, P.; Murillo, C. A.; Timmons, D. J. *Inorg. Chem. Commun.* **2002**, *5*, 501.
(6) Cotton, F. A.; Huang, P.; Murillo, C. A.; Wang, X. *Inorg. Chem. Commun.* **2003**, *6*, 121.
(7) Clérac, R.; Cotton, F. A.; Daniels, L. M.; Donahue, J. P.; Murillo, C. A.; Timmons, D. J. *Inorg. Chem.* **2000**, *39*, 2581.
(8) (a) Eglin, J. L. In *Multiple Bonds between Metal Atoms*, 3rd ed.; Cotton, F. A.; Murillo, C. A.; Walton, R. A. Eds.; Springer Science and Business Media, Inc.: New York, 2005. (b) Eglin, J. L.; Smith, L. T.; Staples, R. J. *Inorg. Chim. Acta* **2003**, *351*, 217.
(9) (a) Collins, D. M.; Cotton, F. A.; Koch, S. A.; Millar, M.; Murillo, C. A. *Inorg. Chem.* **1978**, *17*, 2017. (b) Cotton, F. A.; Mott, G. N.; Schrock, R. R.; Sturgeoff, L. G. *J. Am. Chem. Soc.* **1982**, *104*, 6781.
(10) (a) Chisholm, M. H.; McInnes, J. M. *J. Chem. Soc., Dalton Trans.* **1997**, 2735. (b) Cotton, F. A.; Dikarev, E. V.; Gu, J.; Herrero, S.; Modec, B. *Inorg. Chem.* **2000**, *39*, 5407.
(11) Santure, D. J.; Sattelberger, A. P. *Inorg. Synth.* **1999**, *26*, 219.
(12) Carlson-Day, K. M.; Eglin, J. L.; Smith, L. T.; Staples, R. J. *Inorg. Chem.* **1999**, *38*, 2216.
(13) Chisholm, M. H.; Gallucci, J.; Hadad, C. M.; Huffman, J. C.; Wilson, P. J. *J. Am. Chem. Soc.* **2003**, *125*, 16040.
(14) Cotton, F. A.; Fanwick, P. E.; Niswander, R. H.; Sekutowski, J. C. *J. Am. Chem. Soc.* **1978**, *100*, 4725.
(15) Cotton, F. A.; Ilsley, W. H.; Kaim, W. *Inorg. Chem.* **1980**, *19*, 1453.
(16) Cotton, F. A.; Niswander, R. H.; Sekutowski, J. C. *Inorg. Chem.* **1979**, *18*, 1152.
(17) Kim, J. C.; Goedken, V. L.; Lee, B. M. *Polyhedron* **1996**, *15*, 57.
(18) Cotton, F. A.; Donahue, J. P.; Hall, M. B.; Murillo, C. A.; Villagrán, D. *Inorg. Chem.* **2004**, *43*, 6954.
(19) Cotton, F. A.; Matonic, J. H.; Murillo, C. A. *J. Am. Chem. Soc.* **1998**, *120*, 6047.
(20) Cotton, F. A.; Gu, J.; Murillo, C. A.; Timmons, D. J. *J. Am. Chem. Soc.* **1998**, *120*, 13280.

Scheme 2. Reported Methods for the Preparation of $W_2(hpp)_4$

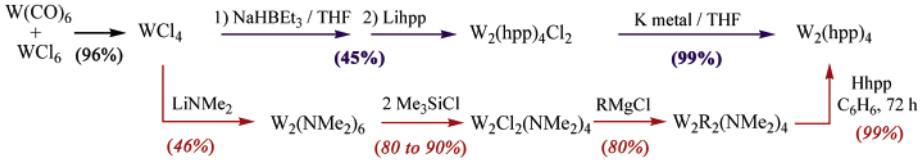

Chart 1. Numerical Designations for Compounds

$W(Hhpp)_2(CO)_4$	**1**
$W_2(\mu\text{-}CO)_2(\mu\text{-}hpp)_2(\eta^2\text{-}hpp)_2$	**2**
$[W_2(\mu\text{-}CO)_2(\mu\text{-}hpp)_2(\eta^2\text{-}hpp)_2]PF_6$	**3**
$W_2(hpp)_4Cl_2$	**4**
$W_2(hpp)_4(PF_6)_2$	**5**
$[W_2(hpp)_4](TFPB)_2$	**6**

case when group-6 metal carbonyls react with amidines.[21,22] We therefore carried out our work in such a way as to be alert for such products in the reaction between the commercially available and stable compounds, $W(CO)_6$ and Hhpp, and we now expand the description of work provided in an initial communication[23] describing a one-pot reaction in *o*-dichlorobenzene that produces the $W_2(hpp)_4$ precursor, $W_2(hpp)_4Cl_2$, in more than 90% yield at 200 °C. We also report two soluble $W_2(hpp)_4^{2+}$ species (see Chart 1) and other W−hpp compounds, some of which may also be obtained by reaction of $W(CO)_6$ with Hhpp at temperatures below 200 °C. The latter provide insight into the reaction pathway leading to the highly insoluble compound $W_2(hpp)_4Cl_2$. Finally, we provide electrochemical studies that show how strongly the bicyclic hpp ligand stabilizes high oxidation states in dimetal units and a comparison of the PES of $W_2(O_2CCH_3)_4$, W_2(diphenylformamidinate)$_4$, and $W_2(hpp)_4$.

Experimental Section

Materials and Methods. Syntheses were carried out under N_2 in a Schlenk line equipped with a mercury bubbler with a height of ca. 4 cm of Hg with a tube diameter of 2.54 cm. Manipulations prior to spectroscopic measurements were conducted under N_2 in a drybox. Acetonitrile was twice distilled under N_2, first from activated molecular sieves and then from CaH_2. Dichloromethane was dried and distilled from P_2O_5. Other solvents such as THF, Et_2O, benzene, and hexanes were either distilled from Na/K−benzophenone or were dried and degassed with a Glass Contour solvent purification system. Chlorobenzene and *o*-dichlorobenzene were dried over freshly activated molecular sieves and degassed with vigorous N_2 bubbling immediately prior to use. Tungsten hexacarbonyl, 1,3,4,6,7,8-hexahydro-*2H*-pyrimido[1,2-*a*]pyrimidine (Hhpp), and $TlPF_6$ were purchased from commercial sources; Hhpp was purified by sublimation, and $TlPF_6$ was dried under vacuum before use. The salt K^+TFPB^- ($TFPB^-$ = tetrakis[3,5-bis(trifluoromethyl)phenyl]borate) was prepared according to a literature procedure.[24]

Physical Methods. Elemental analyses were performed by either Canadian Microanalytical Service, Delta, British Columbia, Canada (for compounds **1**−**3** and **6**) or Robertson Microlit, New Jersey (for compounds **4** and **5**), upon crystalline samples that were redissolved in CH_2Cl_2 and dried overnight under vacuum. ^1H NMR spectra were recorded on a Varian XL-200AA spectrometer with chemical shifts referenced to the protonated solvent residual. Absorption spectra were measured at room temperature under N_2 using a Shimadzu UV-2501 PC spectrophotometer. The cyclic voltammograms (CVs) for **2** and differential pulse voltammograms for **6** were taken with a CH Instruments model-CHI620A electrochemical analyzer in 0.1 M Bu_4NPF_6 solution in CH_2Cl_2 and THF, respectively, using Pt working and auxiliary electrodes, a Ag/AgCl reference electrode, and a scan rate of 100 mV/s for the CVs. All the potential values are referenced to the Ag/AgCl electrode, and under the present experimental conditions, the $E_{1/2}$ for the Fc^+/Fc couple consistently occurred at +440 mV.

X-Ray Structure Determinations. The compounds described in this report are referred to by the numerical designations listed in Chart 1. For **3**−**6**, these numbers specify the complete salt and not merely the ditungsten cation. Yellow block crystals of **1**, needle-shaped crystals of **2**·$2CH_2Cl_2$ (dark red), dark brown plate crystals of **3**·CH_2Cl_2, and dark green-brown plate-crystals of **6** were grown over a period of several days by layering CH_2Cl_2 solutions (5−10 mL) with several portions of hexanes (40−50 mL). Brownish-green block-shaped crystals of **5**·2MeCN·Et_2O were obtained by a similar procedure using a MeCN solution layered with Et_2O. All crystals were coated with Paratone oil and mounted on a quartz fiber or a nylon Cryoloop affixed to a goniometer head. All diffraction data were collected using a Bruker SMART 1000 CCD area detector system using ω scans of 0.3 deg/frame with 30, 60, or 90 s frames such that 1271 frames were collected for a full hemisphere of data. The first 50 frames were recollected at the end of the data collection to monitor for crystal decay, but no significant decomposition was observed. Cell parameters were determined using the program SMART.[25] Data reduction and integration were performed with the software package SAINT,[26] which corrects for Lorentz and polarization effects, while absorption corrections were applied by using the program SADABS.[25]

Space groups for all the compounds structurally characterized by X-ray crystallography were initially determined with the aid of the program XPREP, which is part of the SHELX software package.[27] Compound **1** was uniquely identified as belonging to *Pbcn* by its systematic absences. Good initial solutions and well-behaved refinements for **2**·$2CH_2Cl_2$ and **6** were obtained in $P\bar{1}$ and led us to prefer it over noncentrosymmetric *P*1. For **3**·CH_2Cl_2, the intensity statistics for the data were unclear in suggesting a centric vs noncentric space group. Solution and refinement in $P2_1$ as a

(21) Boeré, R. T.; Klassen, V.; Wolmershäuser, G. *J. Chem. Soc., Dalton Trans.* **1998**, 4147.
(22) de Roode, W. H.; Vrieze, K.; Koerner von Gustorf, E. A.; Ritter, A. *J. Organomet. Chem.* **1977**, *135*, 183.
(23) Cotton, F. A.; Donahue, J. P.; Lichtenberger, D. L.; Murillo, C. A.; Villagrán, D. *J. Am. Chem. Soc.* **2005**, *127*, 10808.
(24) Buschmann, W. E.; Miller, J. S.; Bowman-James, K.; Miller, C. N. *Inorg. Synth.* **2002**, *33*, 83.
(25) *SMART for Windows NT*, Version 5.618; Bruker Analytical X-ray Systems: Madison, WI, 2000.
(26) *SAINT+ for NT*, Version 6.28A.; Bruker Analytical X-ray Systems: Madison, WI, 2001.
(27) Sheldrick, G. M. *SHELX-97 Programs for Crystal Structure Analysis*; Institüt für Anorganische Chemie der Universität, Tammanstrasse 4, D-3400 Göttingen, Germany, 1998.

Table 1. Crystallographic Data for Tungsten−hpp Compounds

compound	**1**	**2**·2CH_2Cl_2	**3**·CH_2Cl_2	**6**
formula	$C_{18}H_{26}N_6O_4W$	$C_{32}H_{52}Cl_4N_{12}O_2W_2$	$C_{31}H_{50}Cl_2F_6N_{12}O_2PW_2$	$C_{92}H_{72}B_2F_{48}N_{12}W_2$
fw, g·mol^{-1}	574.30	1146.36	1206.40	2646.94
cryst syst	orthorhombic	triclinic	monoclinic	triclinic
space group	*Pbcn*	$P\bar{1}$	$P2_1$	$P\bar{1}$
a (Å)	7.6069(7)	9.1469(9)	8.7824(8)	13.2001(2)
b (Å)	16.320(2)	10.821(1)	15.731(1)	14.863(2)
c (Å)	16.667(2)	11.896(1)	14.383(1)	26.035(3)
α (deg)	90	102.471(2)	90	87.365(2)
β deg)	90	101.692(2)	94.850(2)	88.944(2)
γ (deg)	90	114.904(2)	90	76.617(2)
V (Å^3)	2069.2(3)	983.8(2)	1980.0(3)	4964(1)
Z	4	1	2	2
d_{calc} (g·cm^{-1})	1.844	1.935	2.204	1.711
μ (mm^{-1})	5.620	6.161	6.057	2.459
2*θ* (deg)	4.9−55.1	4.4−55.0	3.8−55.1	3.2−55.1
λ, Å	0.71073	0.71073	0.71073	0.71073
T, °C	−60	−60	−60	−60
GOF	1.107	1.029	1.020	1.019
R1,[a] wR2($I > 2\sigma(I)$)	0.018, 0.044	0.027, 0.068	0.028, 0.060	0.041, 0.095

[a] $R1 = \sum||F_o| - |F_c||/\sum|F_o|$. [b] $wR2 = [\sum[w(F_o^2-F_c^2)^2]/\sum w(F_o^2)^2]^{1/2}$, $w = 1/[\sigma^2(F_o^2) + (aP)^2 + bP]$, where $P = [\max(F_o^2 \text{ or } 0) + 2(F_c^2)]/3$.

slight racemic twin (Flack parameter = 0.10) yielded a decidedly better refinement with lower residuals than did refinement in $P2_1/a$, the most plausible centrosymmetric alternative. The space group for **5**·2MeCN·Et_2O was not entirely unambiguous, but following the arguments advanced by Marsh,[28] *I*4/*mmm* was preferred because it was the space group of highest symmetry consistent with good refinement of the data.

In all structures, the positions of the W atoms or other heavy atoms were found via direct methods using the SHELX software.[27] The positions of the remaining non-hydrogen atoms were revealed by subsequent cycles of least-squares refinement followed by difference Fourier syntheses. In **3**·CH_2Cl_2, the PF_6^- anion was disordered over two slightly offset orientations and was refined as an optimal distribution between these two positions with appropriate constraints on the P−F and nonbonded F···F distances. One chlorine atom of the interstitial CH_2Cl_2 molecule in this crystal structure was also disordered over two sets of coordinates and modeled accordingly. The solvent that crystallized with **5** was modeled as a superposition of two molecules of MeCN and one of Et_2O with chemically reasonable constraints imposed on the bond distances. In the $TFPB^-$ anions in **6**, most of the CF_3 groups were disordered over two or three rotational positions and refined as a best-fit distribution between these positions as determined by the refinement software. In **1**, the hydrogen atoms were visible in the final electron density maps, and their positions were accordingly refined. For **2**·2CH_2Cl_2, most but not all of the hydrogen atom positions were refined. In the remaining compounds, hydrogen atoms were added in calculated positions and treated as riding atoms with isotropic displacement parameter values equal to 1.2 times those of the carbon atoms to which they were attached. Cell parameters and refinement results for all compounds are summarized in Table 1[29] while selected metric parameters are collected in Tables 2−5.

Photoelectron Spectroscopy. The gas-phase PES of $W_2(hpp)_4$ was recorded using an instrument that features a 36-cm radius, 8-cm gap hemispherical analyzer,[30] and custom-designed excitation source, sample cells, detection and control electronics, and methods that have been described in detail previously.[31,32] The temperature was monitored using a "K"-type thermocouple passed through a vacuum feedthrough and attached directly to the sample cell. Samples were loaded into the cell and placed in the instrument using rigorous air-sensitive techniques and were vaporized by controlled temperature ramping while monitoring the gas-phase PES for purity before data collection. The only volatile contaminant

Table 2. Bond Parameters (Å or deg) for **1**

W(1)−C(1)	2.030(3)	O(1)−C(1)−W(1)	172.6(2)
W(1)−C(2))	1.951(3)	O(2)−C(2)−W(1)	177.4(2)
W(1)−N(1)	2.295(2)	O(1)−W(1)−C(2)	86.0(1)
C(1)−O(1)	1.151(3)	C(1)−W(1)−C(1A)	171.1(1)
C(2)−O(2)	1.168(3)	C(2)−W(1)−C(2A)	87.0(2)
N(1)−C(3)	1.317(3)	N(1)−W(1)−N(1A)	87.8(1)
N(2)−C(3)	1.366(3)	N(1)−C(3)−N(2)	117.6(2)
N(3) C(3)	1.353(3)	N(1)−C(3)−N(3)	125.0(2)
		N(2)−C(3)−N(3)	117.5(2)

Table 3. Bond Parameters (Å or deg) for **2**

W(1)−W(1A)	2.4675(3)	W(1)−C(1)−W(1A)	70.6(1)
W(1)−N(1)	2.138(3)	W(1)−C(1)−O(1)	167.0(3)
W(1)−N(2A)	2.128(3)	W(1A)-C(1)−O(1)	122.4(3)
W(1)−N(4)	2.153(4)	N(1)−W(1)−N(2A)	172.4(1)
W(1)−N(5)	2.181(3)	C(1)−W(1)−W(1A)	61.3(1)
W(1)−C(1)	1.944(4)	C(1)−W(1A)-W(1)	48.03(9)
W(1)−C(1A)	2.294(4)	N(4)−W(1)−C(1)	94.3(2)
C(1)−O(1)	1.188(5)	N(5)−W(1)−C(1)	155.5(2)
N(1)−C(2)	1.349(5)	N(1)−C(2)−N(2)	119.5(3)
N(2)−C(2)	1.357(5)	N(4)−C(9)−N(5)	111.8(4)

Table 4. Bond Parameters (Å or deg) for the Cation in **3**

W(1)−W(2)	2.5096(3)	W(1) −C(1)−O(1)	166.9(6)
W(1)−C(1)	1.985(6)	W(1)−C(2)−O(2)	122.8(5)
W(1)−C(2)	2.344(7)	W(2)−C(1)−O(1)	122.6(5)
W(2)−C(1)	2.339(7)	W(2)−C(2)−O(2)	167.0(6)
W(2)−C(2)	1.987(7)	C(1)−W(1)−W(2)	61.4(2)
C(1)−O(1)	1.168(7)	C(1)−W(2)−W(1)	48.2(1)
C(2)−O(2)	1.172(7)	N(1)−W(1)−N(10)	172.0(3)
W−N(*μ*), av	2.104(4)	N(4)−W(1)−N(5)	63.5(2)
W−N(*η*), av	2.117(3)	N(5)−W(1)−C(1)	158.1(3)

(28) Marsh, R. E. *Acta Crystallogr.* **1986**, *B42*, 193.
(29) Crystallographic data for **5**·2MeCN·Et_2O are as follows: Space group = *I*4/*mmm*, *a* = *b* = 11.707(1) Å, *c* = 17.856(4) Å, *V* = 2447.4(7) Å^3, *Z* = 2, R1 = 0.018, wR2 = 0.054. Additional crystallographic data are provided as Supporting Information.
(30) Siegbahn, K.; Nordling, C.; Fahlman, A.; Nordberg, R.; Hamrin, K.; Hedman, J.; Johansson, G.; Bergmark, T.; Karlsson, S.-E.; Lindgren, I.; Lindberg, B. *Atomic, Molecular and Solid State Structure Studied by Means of Electron Spectroscopy*; Almqvist and Wiksells: Uppsala, 1967.
(31) Lichtenberger, D. L.; Kellogg, G.; Kristofzski, J. G.; Page, D.; Turner, S.; Klinger, G.; Lorenzen, J. *Rev. Sci. Instrum.* **1986**, *57*, 2366.
(32) Westcott, B. L.; Gruhn, N. E.; Enemark, J. H. *J. Am. Chem. Soc.* **1998**, *120*, 3382 and references therein.

Table 5. Bond Parameters (Å or deg) for the Cation in **6**

W(1)−W(2)	2.1920(3)	N(1)−W(1)−N(4)	90.9(2)
W(1)−N(1)	2.078(4)	N(1)−W(1)−N(7)	176.0(2)
W(2)−N(2)	2.071(4)	N(1)−W(1)−N(10)	89.1(2)
W(1)−N(4)	2.071(4)	N(4)−W(1)−N(7)	90.9(2)
W(2)−N(5)	2.085(4)	N(4)−W(1)−W(10)	177.0(2)
W(1)−N(7)	2.074(4)	N(7)−W(1)−N(10)	89.0(2)
W(2)−N(8)	2.079(4)	N(2)−W(2)−N(5)	88.8(2)
W(1)−N(10)	2.089(4)	N(2)−W(2)−N(8)	175.8(2)
W(2)−N(11)	2.064(4)	N(2)−W(2)−N(11)	90.4(2)

observed was a small amount of Hhpp,[33] with the actual amount observed varying from sample to sample. The spectrum of Hhpp would be observed beginning at about 40 °C; the temperature would be held at this point until all Hhpp was gone, and then controlled temperature ramping would resume. $W_2(hpp)_4$ sublimes under our instrument conditions beginning at 230 °C, and the sample was heated as high as 300 °C with no sign of decomposition.

The argon $^2P_{3/2}$ ionization at 15.759 eV and the He self-ionization with He II photons, which appears at an apparent ionization energy of 4.99 eV in the He I spectrum, were used as internal calibration locks of the absolute ionization energy. The difference between the argon $^2P_{3/2}$ ionization and the methyl iodide $^2E_{1/2}$ ionization at 9.538 eV was used to calibrate the energy scale. During data collection, the instrument resolution (measured using the full-width at half maximum of the argon $^2P_{3/2}$ peak) was better than 0.040 eV. Vertical ionization energies are defined by the position of asymmetric Gaussians[34] used to analytically model the shape of the ionization features. On the basis of our experience with this spectroscopic technique and the shapes of the ionization bands, vertical ionization energies are reproducible to ±0.02 eV (3σ level).

Computational Details. Density functional theory (DFT)[35] calculations were performed with the hybrid Becke 3-parameter exchange functional[36] and the Lee−Yang−Parr nonlocal correlation functional[37] (B3LYP) implemented in the Gaussian 03 (Revision C.02) program suite.[38] Double-ζ quality basis sets (D95)[39a] were used on carbon, nitrogen, and hydrogen atoms as implemented in Gaussian. Chlorine atoms were described by the effective core potential (ECP) by Hay and Wadt (LANL2DZ).[40] A version of Hay and Wadt's ECP[40b] modified by Couty and Hall,[41] and augmented by an *f* polarization function[42] was used for the tungsten atoms. Fragment analysis of the wave function was accomplished by expressing the Gaussian output in the Kohn−Sham matrix form of the type $H_{KS}C = SCE$, where H_{KS} is the Kohn−Sham Hamiltonian matrix, C is the eigenvector matrix, S is the overlap matrix, and E is the diagonal eigenvalue matrix,[43] with the matrixes transformed to the basis of the $[W_2(hpp)_4]^{2+}$ and $[2Cl]^{2-}$ fragments using the calculated coordinates for the $W_2(hpp)_4Cl_2$ molecule. To gain insight into the electronic transitions responsible for the observed UV−vis spectra of **5** and **6**, time-dependent density functional theory[44] (TD-DFT) calculations were performed using the Gaussian program suite. All calculations were run on an Origin 3800 64-processor SGI computer located at the Texas A&M Supercomputing facility.

Syntheses. W(Hhpp)$_2$(CO)$_4$ (1). A solution of $W(CO)_6$ (0.386 g, 1.10 mmol) and Hhpp (0.300 g, 2.16 mmol) in 50 mL of chlorobenzene was heated under N_2 to 120 °C for 3 h. After cooling to ambient temperature, the yellow-orange solution was evaporated to dryness under reduced pressure and extracted with 2 × 6 mL of CH_2Cl_2. These extracts were filtered and then layered with 50 mL of hexanes. After several days, the yellow block-crystals of **1** were collected and dried under vacuum. Yield: 0.428 g, 68%. ^{1}H NMR δ (in CD_2Cl_2): 5.67 (broad s, 2H, N−*H*), 3.41 (t, 4H, N−C*H*$_2$), 3.25 (m, 4H, N−C*H*$_2$), 3.15 (m, 8H, N−C*H*$_2$), 1.91 (quintet, 4H, −CH$_2$C*H*$_2$CH$_2$−), 1.77 (m, 4H, −CH$_2$C*H*$_2$CH$_2$−). IR (KBr, cm^{-1}): 1863 (vs, ν_{CO}), 1840 (vs, ν_{CO}), 1780 (vs, ν_{CO}). Absorption spectrum (CH_2Cl_2) λ_{max} (ϵ_M): 297 (8310), 396 (2010). Anal. Calcd for $C_{18}H_{26}N_6O_4W$: C, 37.65; H, 4.56; N, 14.63. Found: C, 37.55; H, 4.38; N, 14.61.[45]

W$_2$(μ-CO)$_2$(μ-hpp)$_2$(η^2-hpp)$_2$ (2). A solution of $W(CO)_6$ (0.250 g, 0.71 mmol) and Hhpp (0.270 g, 1.94 mmol) in 35 mL of a 6:1 mixture of *o*-dichlorobenzene/hexanes[46] was heated to 180 °C for 24 h under N_2. The resulting dark green-blue mixture was cooled to ambient temperature, filtered, and evaporated to dryness under reduced pressure. The remaining dark residue was washed with 2 × 50 mL of distilled, degassed H_2O, and the dull blue solid was thoroughly dried under vacuum. Extraction of this blue solid with CH_2Cl_2 (3 × 20 mL), filtration, and evaporation of the filtrate to dryness under reduced pressure yielded a dark blue, microcrystalline solid. Yield: 0.185 g, 53%. ^{1}H NMR δ (in CD_2Cl_2): 3.68 (m, 8H, N−C*H*$_2$), 3.43 (t, 8H, N−C*H*$_2$), 3.05 (m, 16H, N−C*H*$_2$), 1.99 (m, 8H, −CH$_2$C*H*$_2$CH$_2$−), 1.80 (quintet, 8H, −CH$_2$C*H*$_2$CH$_2$−). IR (KBr, cm^{-1}): 1708 (vs, ν_{CO}). Absorption spectrum (CH_2Cl_2) λ_{max} (ϵ_M): 313 (25 500), 427 (sh, 1560), 618 (1380). ESI-MS: *m*/*z* 976 (M^+), 920 (M^+ − 2CO). Anal. Calcd for W$_2$(μ-CO)$_2$(μ-hpp)$_2$(η^2-hpp)$_2$·$^1/_2$CH$_2$Cl$_2$, $C_{30.5}H_{49}ClN_{12}O_2W_2$: C, 35.95; H, 4.85; N, 16.50. Found: C, 36.17; H, 4.97; N, 16.58. Solutions of **2** in CH_2Cl_2 were very sensitive to air.

[W$_2$(μ-CO)$_2$(μ-hpp)$_2$(η^2-hpp)$_2$]PF$_6$ (3). To a solution of W$_2$(μ-CO)$_2$(μ-hpp)$_2$(η^2-hpp)$_2$ (0.204 g, 0.209 mmol) in 50 mL of CH_2Cl_2 was added crystalline $(Cp_2Fe)PF_6$ (0.069 g, 0.208 mmol) under a

(33) Novak, I.; Wei, X.; Chin, W. S. *J. Phys. Chem. A* **2001**, *105*, 1783.
(34) Lichtenberger, D. L.; Copenhaver, A. S. *J. Electron Spectrosc. Relat. Phenom.* **1990**, *50*, 335.
(35) (a) Hohenberg, P.; Kohn, W. *Phys. Rev.* **1964**, *136*, B864. (b) Parr, R. G.; Yang, W. *Density-Functional Theory of Atoms and Molecules*; Oxford University Press: Oxford, 1989.
(36) (a) Becke, A. D. *Phys. Rev. A* **1988**, *38*, 3098. (b) Becke, A. D. *J. Chem. Phys.* **1993**, *98*, 1372. (c) Becke, A. D. *J. Chem. Phys.* **1993**, *98*, 5648.
(37) Lee, C.; Yang, W.; Parr, R. G. *Phys. Rev. B* **1988**, *37*, 785.
(38) Frisch, M. J.; Trucks, G. W.; Schlegel, H. B.; Scuseria, G. E.; Robb, M. A.; Cheeseman, J. R.; Montgomery, J. A., Jr.; Vreven, T.; Kudin, K. N.; Burant, J. C.; Millam, J. M.; Iyengar, S. S.; Tomasi, J.; Barone, V.; Mennucci, B.; Cossi, M.; Scalmani, G.; Rega, N.; Petersson, G. A.; Nakatsuji, H.; Hada, M.; Ehara, M.; Toyota, K.; Fukuda, R.; Hasegawa, J.; Ishida, M.; Nakajima, T.; Honda, Y.; Kitao, O.; Nakai, H.; Klene, M.; Li, X.; Knox, J. E.; Hratchian, H. P.; Cross, J. B.; Bakken, V.; Adamo, C.; Jaramillo, J.; Gomperts, R.; Stratmann, R. E.; Yazyev, O.; Austin, A. J.; Cammi, R.; Pomelli, C.; Ochterski, J. W.; Ayala, P. Y.; Morokuma, K.; Voth, G. A.; Salvador, P.; Dannenberg, J. J.; Zakrzewski, V. G.; Dapprich, S.; Daniels, A. D.; Strain, M. C.; Farkas, O.; Malick, D. K.; Rabuck, A. D.; Raghavachari, K.; Foresman, J. B.; Ortiz, J. V.; Cui, Q.; Baboul, A. G.; Clifford, S.; Cioslowski, J.; Stefanov, B. B.; Liu, G.; Liashenko, A.; Piskorz, P.; Komaromi, I.; Martin, R. L.; Fox, D. J.; Keith, T.; Al-Laham, M. A.; Peng, C. Y.; Nanayakkara, A.; Challacombe, M.; Gill, P. M. W.; Johnson, B.; Chen, W.; Wong, M. W.; Gonzalez, C.; Pople, J. A. *Gaussian 03*, revision C.02; Gaussian, Inc.: Wallingford, CT, 2004.
(39) (a) Dunning, T. H.; Hay, P. J. In *Modern Theoretical Chemistry. 3. Methods of Electronic Structure Theory*; Schaefer, H. F., III, Ed.; Plenum Press: New York, 1977; pp 1−28. (b) Woon, D. E.; Dunning, T. H. *J. Chem. Phys.* **1993**, *98*, 1358.
(40) (a) Wadt, W. R.; Hay, P. J. *J. Chem. Phys.* **1985**, *82*, 284. (b) Hay, P. J.; Wadt, W. R. *J. Chem. Phys.* **1985**, *82*, 299.
(41) Couty, M.; Hall, M. B. *J. Comput. Chem.* **1996**, *17*, 1359.
(42) Hollwarth, A.; Bohme, M.; Dapprich, S.; Ehlers, A. W.; Gobbi, A.; Jonas, V.; Kohler, K. F.; Stegmann, R.; Veldkamp, A.; Frenking, G. *Chem. Phys. Lett.* **1993**, *208*, 111.
(43) Senthilkumar, K.; Grozema, F. C.; Bickelhaupt, F. M.; Siebbeles, L. D. A. *J. Chem. Phys.* **2003**, *119*, 9809.
(44) Casida, M. E.; Jamorski, C.; Casida, K. C.; Salahub, D. R. *J. Chem. Phys.* **1998**, *108*, 4439.

(45) These values represent the average of two separate analyses performed upon the same sample.
(46) The use of hexanes is useful to prevent the reaction temperature from becoming too high and leading to formation of $W_2(hpp)_4Cl_2$.

N_2 flow. The dark blue-violet color of $W_2(\mu\text{-}CO)_2(\mu\text{-}hpp)_2(\eta^2\text{-}hpp)_2$ turned a deep, dark-green color. Stirring at room temperature was continued for 2 h, and the CH_2Cl_2 was then removed under vacuum. The resulting brown residue was washed with 3 × 10 mL of Et_2O to remove the byproduct Cp_2Fe. The product was extracted with 3 × 4 mL of CH_2Cl_2, and these extracts were then filtered and layered with hexanes. Dark brown-black, plate crystals formed after 72 h. Yield: 0.112 g, 48%. IR (KBr, cm^{-1}): 1758 (vs, ν_{CO}). Absorption spectrum (CH_2Cl_2) λ_{max} (ϵ_M): 263 (sh, 10 900) 323 (15 400), 356 (11 100), 406 (sh, 6260), 652 (894). ESI-MS: *m*/*z* 976 (M^+), 920 ($M^+ - 2CO$). Anal. Calcd for $C_{30}H_{48}F_6N_{12}O_2PW_2$: C, 32.13; H, 4.31; N, 14.89. Found: C, 32.05; H, 4.54; N, 14.39.

$W_2(hpp)_4Cl_2$ (4). This was prepared similarly to **2** but using higher reflux temperatures by eliminating the addition of hexanes. An oven-dried 100-mL Schlenk flask was charged with a stir bar, 1.00 g (2.84 mmol) of $W(CO)_6$, 0.90 g (6.47 mmol) of Hhpp, and 30 mL of degassed *o*-dichlorobenzene. The flask was then fitted with a water-cooled coldfinger. This mixture was vigorously refluxed under N_2 at 200 °C for 8 h and then cooled to ambient temperature. The brown-green precipitate that formed was collected by filtration and washed with 3 × 15 mL of CH_2Cl_2. Yield: 1.29 g, 92%. Anal. Calcd for $C_{28}H_{48}N_{12}Cl_2W_2$: C, 33.92; H, 4.88; N, 16.95. Found: C, 33.80; H, 4.69; N, 16.59. The ^1H NMR spectrum and other spectroscopic characteristics were the same as those reported earlier.[7]

$W_2(hpp)_4(PF_6)_2$ (5). $TlPF_6$ was dried overnight under vacuum at 110 °C. An oven-dried 100-mL Schlenk flask was charged with a stir bar, 0.200 g (0.200 mmol) of $W_2(hpp)_4Cl_2$, 0.140 g (0.400 mmol) of $TlPF_6$, and 15 mL of degassed acetonitrile. The resulting suspension was stirred vigorously for 8 h, during which time a red solution with a white precipitate formed. The red solution was filtered through Celite and then layered with Et_2O. After several days, large red crystals suitable for X-ray crystallography were obtained. Yield: 0.113 g, 53%. Absorption spectrum (CH_2Cl_2) λ_{max} (ϵ_M): 270 (7800), 293 (sh, 4600), 359 (8760). ^1H NMR δ (in CD_2Cl_2): 3.44 (t, 16H, N−C*H*$_2$), 3.35 (t, 16H, N−C*H*$_2$), 2.00 (quintet, 16H, −CH_2C*H*$_2$C*H*$_2$−). Anal. Calcd for $C_{28}H_{48}F_{12}N_{12}P_2W_2$: C, 27.78; H, 4.00; N, 13.89. Found: C, 27.41; H, 3.70; N, 13.58.

$[W_2(hpp)_4](TFPB)_2$ (6). A 100-mL Schlenk flask was charged with 0.100 g (0.100 mmol) of $W_2(hpp)_4Cl_2$, 0.180 g (0.200 mmol) of K^+(TFPB), and 15 mL of CH_2Cl_2. The resulting suspension was stirred for 8 h. The red solution was filtered through Celite and layered with 50 mL of isomeric hexanes. Large green-brown crystals suitable for X-ray crystallography were obtained in 48−72 h. Yield: 0.147 g, 55%. Absorption spectrum (CH_2Cl_2) λ_{max} (ϵ_M): 269 (33 000), 280 (sh, 25 000), 361 (33 000). ESI^+-MS: *m*/*z* 460 (M^{2+}/2). Anal. Calcd for $C_{92}H_{72}B_2H_{48}N_{12}W_2$: C, 41.75; H, 2.74; N, 6.35. Found: C, 41.32; H, 2.91; N, 6.65.

Results and Discussion

Syntheses and Structures. The chief results of this work are (1) a new synthetic route to $W_2(hpp)_4Cl_2$ that proceeds in a one-pot reaction at 200 °C from the readily available starting materials, $W(CO)_6$ and Hhpp in *o*-dichlorobenzene, in greater than 90% isolated yield and (2) a more definitive PES of $W_2(hpp)_4$.

The new synthetic route constitutes a huge improvement over both previously reported routes[7] in terms of time, convenience, purity, and cost. Since the conversion of $W_2(hpp)_4Cl_2$ to $W_2(hpp)_4$ is also simple and efficient, the way is now open for productive exploration of the chemistry of $W_2(hpp)_4$, a compound that ionizes easily but is stable in a vacuum to at least 300 °C.

In addition to the excellent route for preparation of $W_2(hpp)_4Cl_2$, a considerable amount of related chemistry has been turned up by our studies of the reactions of $W(CO)_6$ with Hhpp under various conditions. With reaction times of less than 15 h at or below a reaction temperature of 150 °C, an ill-defined mixture of species is produced from which yellow $W(Hhpp)_2(CO)_4$ (**1**) is the only identifiable product. This compound may be prepared more deliberately and cleanly from $W(CO)_6$ under less-forcing conditions. Its structure, a classic octahedron with cis-oriented Hhpp ligands, is presented in Figure 1 with accompanying selected metric parameters in Table 2.[47,48] Such mononuclear molybdenum and tungsten carbonyl complexes with amine- and imine-type ligands are abundantly precedented in the chemical literature,[49] but we note that molybdenum complexes of this type where the nitrogen ligand is an amidine generally result either from mild reaction[21] conditions or because the steric demands of the amidine ligand obviate formation of dimetal products.

More vigorous reaction conditions (24 h, ∼180 °C) produce good yields of a dull blue solid which has been identified as the edge-sharing bioctahedral molecule $W_2(\mu\text{-}CO)_2(\mu\text{-}hpp)_2(\eta^2\text{-}hpp)_2$ (**2**). The isolation of both **1** and **2** from the same reaction mixture, when shortened reaction times and lowered temperatures are used, suggests that the former is a precursor to the latter. It is possible that **2** forms by the close approach of two molecules of **1** as illustrated in Scheme 3 and that metal−metal bond formation occurs concomitantly with loss of CO and H_2.[18]

The structure of **2** is shown in Figure 1, and a list of relevant bond lengths and angles is presented in Table 3. This molecule resides on an inversion center in the space group $P\bar{1}$ and has a W−W bond length of 2.4675(3) Å that is clearly indicative of a moderate degree of metal−metal bonding. An important feature in this structure is the highly unsymmetrical nature of the bridging CO ligands, which lowers the molecular symmetry from D_{2h} to C_{2h}. The difference of 0.350(8) Å between the W−C and W−C(1A) bond lengths is quite large. Furthermore, the W(1)−C(1)−O(1) bond angle of 167.0(3)° in **2** approaches the linearity that would be expected for a terminal rather than a bridging CO ligand, while the C(1)−W(1)−W(1A) bond angle is 61.3(1)°. Using the structural criteria described by Crabtree

(47) The isostructural molybdenum compound has also been structurally characterized by X-ray diffraction, and its structure has been included as Supporting Information. Crystallographic data are as follows: Orthorhombic space group *Pbcn*, a = 7.672(1) Å, b = 16.498(3) Å, c = 16.824(3) Å, V = 2129.3(7) Å^3, Z = 4, R1 = 0.074, wR2 = 0.139.

(48) $W(Hhpp)_2(CO)_4$ has been found to crystallize from CH_2Cl_2/hexanes as a polymorph of the crystal reported in Table 1 and presented in Figure 1. Crystallographic data for this polymorph are as follows: Space group = $P2_1/n$, a = 8.0954(9) Å, b = 14.788(2) Å, c = 17.043-(2) Å, $\hat{a}$ = 91.280(2)°, V = 2039.7(4) Å^3, Z = 4, R1 = 0.015, wR2 = 0.035. Additional crystallographic data are provided as Supporting Information.

(49) (a) Darensbourg, D. J.; Kump, R. L. *Inorg. Chem.* **1978**, *17*, 2680. (b) Mentes, A. *Transition Met. Chem.* **1999**, *24*, 77 and references therein.

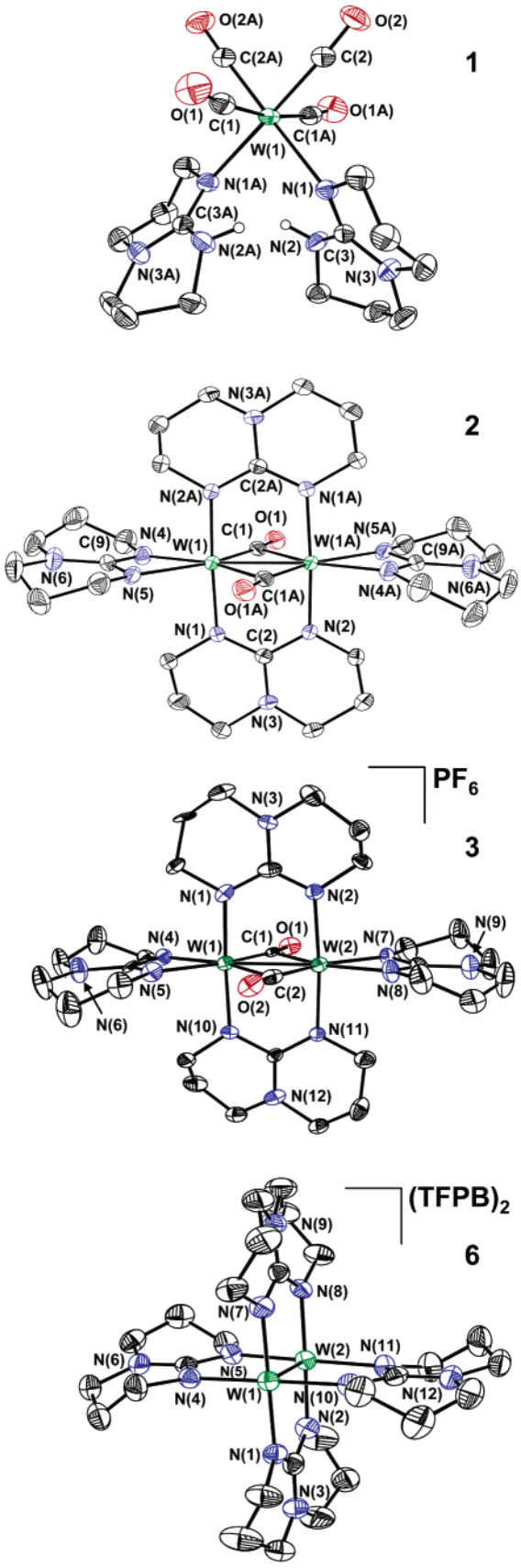

Figure 1. Displacement ellipsoid plots at the 50% probability level for $W(Hhpp)_2(CO)_4$ (**1**), $W_2(\mu\text{-}CO)_2(\mu\text{-}hpp)_2(\eta^2\text{-}hpp)_2$ (**2**), the $[W_2(\mu\text{-}CO)_2(\mu\text{-}hpp)_2(\eta^2\text{-}hpp)_2]^+$ cation in **3**, and the $[W_2(hpp)_4]^{2+}$ dication in **6**. Hydrogen atoms have been removed for clarity.

and Lavin,[50] **2** meets the definition of a Type II linear semibridging carbonyl system.

Compound **2** is analogous to the previously reported[18] ditungsten formamidinate compound, $W_2(\mu\text{-}CO)_2(\mu\text{-}DAniF)_2(\eta^2\text{-}DAniF)_2$. Qualitatively similar structural features are observed in this pair of compounds, but in **2**, the tungsten−tungsten bond distance is shorter (2.4675(3) vs 2.476(1) Å), the skewing of the W−C bond distances within the $W_2(\mu\text{-}CO)_2$ core is greater (1.944(4) and 2.294(4) Å in **2** vs 1.99(1) and 2.28(1) Å in $W_2(\mu\text{-}CO)_2(\mu\text{-}DAniF)_2(\eta^2\text{-}DAniF)_2$), and each μ-CO ligand approaches greater linearity with one of the tungsten atoms (167.0(3)° in **2** vs 163(1)° in $W_2(\mu\text{-}CO)_2(\mu\text{-}DAniF)_2(\eta^2\text{-}DAniF)_2$). DFT calculations[18] on $W_2(\mu\text{-}CO)_2(\mu\text{-}DAniF)_2(\eta^2\text{-}DAniF)_2$ revealed that the basis for the D_{2h}-to-C_{2h} symmetry lowering through skewing of the $W_2(\mu\text{-}CO)_2$ core is due to an enhanced W → CO π^* back-bonding interaction. The same effect is operative in **2** but is even more pronounced because the significantly greater electron-donating capacity of the hpp anion infuses more electron density into the W_2^{4+} unit that in turn is alleviated by enhanced W → CO π^* back-bonding. Stretching frequencies of 1708 and 1747 cm^{-1} in the IR for the μ-CO ligands in **2** and $W_2(\mu\text{-}CO)_2(\mu\text{-}DAniF)_2(\eta^2\text{-}DAniF)_2$) are consistent with greater W → CO π^* back-bonding in **2** and corroborate the interpretation of the structural results. The metal−metal bond order in **2** may be formulated as a double bond as it was in $W_2(\mu\text{-}CO)_2(\mu\text{-}DAniF)_2(\eta^2\text{-}DAniF)_2$).[18]

Although **2** appears relatively stable in the solid state, its solutions readily change color upon exposure to air. A deliberate one-electron oxidation with Cp_2Fe^+ in CH_2Cl_2 induces a color change to an intense, dark green, although the crystalline solid that is isolated appears brown. The salt $[W_2(\mu\text{-}CO)_2(\mu\text{-}hpp)_2(\eta^2\text{-}hpp)_2]PF_6$ (**3**) crystallizes from CH_2Cl_2/hexanes in the noncentric space group $P2_1$ as the dichloromethane monosolvate, but slower crystal growth from the same solvent system produces **3** in space group $C2/c$ without interstitial solvent molecules.[51] The structure of the cation in **3** is presented in Figure 1; it differs from that of **2** in several respects. The tungsten−tungsten bond length in $[W_2(\mu\text{-}CO)_2(\mu\text{-}hpp)_2(\eta^2\text{-}hpp)_2]^+$ is 0.0421(7) Å longer than that in **2**, while the tungsten−carbon bond distances are lengthened by an amount ranging from 0.04 to 0.05 Å. These structural changes are consistent with removal of an electron from a molecular orbital that has both metal−metal bonding and metal-to-CO π^* back-bonding character in **2** (vide infra), but they do not alter the $W_2(\mu\text{-}CO)_2$ core sufficiently to remove the cation in **3** from classification as a Type II linear semibridging carbonyl system.[50] The IR spectrum of **3** (KBr) reveals a ν_{CO} stretching frequency at 1758 cm^{-1} in agreement with the decreased W → CO π^* back-bonding that is indicated by the structural changes observed in going from **2** to **3**.

(50) Crabtree, R. H.; Lavin, M. *Inorg. Chem.* **1986**, *25*, 805.
(51) Crystallographic data for solvent-free **3** are as follows: Space group = $C2/c$, a = 16.611(2) Å, b = 9.125(1) Å, c = 24.082(3) Å, β = 92.341(2)°, V = 3647.4(9) Å^3, Z = 4, R1 = 0.040, wR2 = 0.091. Additional crystallographic data are provided as Supporting Information.

Scheme 3. Proposed Stepwise Formation of **1**, **2**, and **4** from $W(CO)_6$

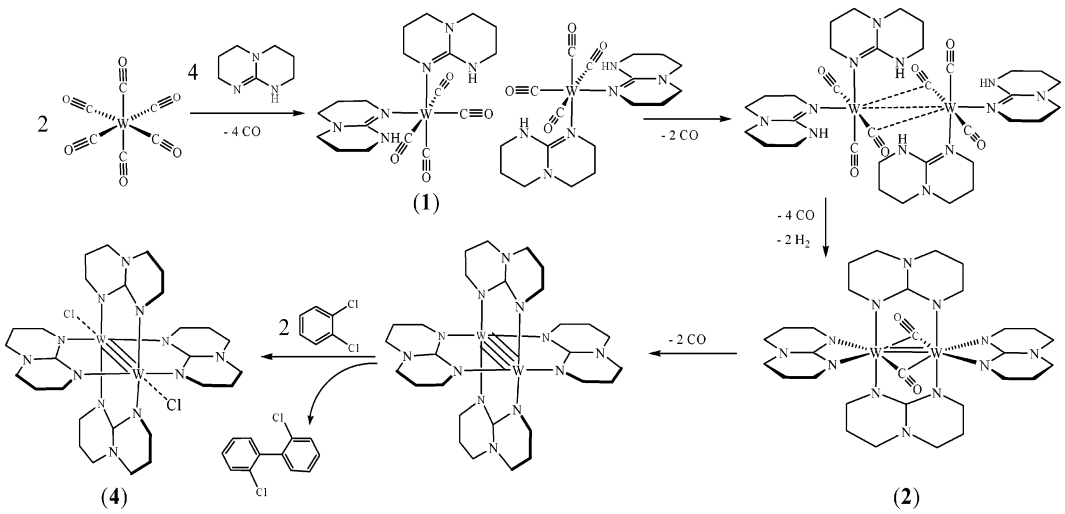

The reaction of $W(CO)_6$ with Hhpp in *o*-dichlorobenzene without added hexanes favors formation of a dark brown sparingly soluble powder that precipitates as the mixture cools. Examination of this material by ^{1}H NMR (DMSO-d_6) revealed a spectrum identical to that previously reported for $W_2(hpp)_4Cl_2$ prepared from WCl_4 (Scheme 2).[7] The generation of $W_2(hpp)_4Cl_2$ may proceed from $W_2(\mu\text{-CO})_2(\mu\text{-hpp})_2(\eta^2\text{-hpp})_2$ by further loss of the two bridging CO ligands along with rearrangement of the two η^2-hpp ligands into a bridging mode to give $W_2(hpp)_4$, as suggested in Scheme 3. Additional support for this reaction pathway is found in the ESI$^+$ mass spectrum of $W_2(\mu\text{-CO})_2(\mu\text{-hpp})_2(\eta^2\text{-hpp})_2$, which displays, in addition to a prominent parent ion peak, a smaller peak corresponding to $W_2(hpp)_4$ after loss of the two CO ligands (Figure 2). The transient $W_2(hpp)_4$ thus formed under the harsh conditions of refluxing *o*-dichlorobenzene immediately reacts with the aryl chloride solvent to produce the oxidized $W_2(hpp)_4Cl_2$ compound[52] and 2,2′-dichlorobiphenyl as the reduced species. The byproduct 2,2′-dichlorobiphenyl was detected by GC-MS in the reaction filtrate after isolation of $W_2(hpp)_4Cl_2$.

The sparing solubility of $W_2(hpp)_4Cl_2$ in common organic solvents has led us to seek exchange of the chloride anions for other counterions that would render $[W_2(hpp)_4]^{2+}$ more soluble. Stirring a suspension of $W_2(hpp)_4Cl_2$ with either $TlPF_6$ or with K^+TFPB^- produces a white precipitate of either TlCl or KCl and a homogeneous red supernatant from which the $[W_2(hpp)_4]^{2+}$ species may be crystallized with the corresponding anion. In **5**, both the $[W_2(hpp)_4]^{2+}$ unit and the PF_6^- anions reside upon a 4-fold axis in the space group *I*4/*mmm* while each of the six-membered rings in each hpp ligand is disordered between two different buckled conformations. The W···F separation is 2.774(5) Å. In **6**, there are no close contacts between the $[W_2(hpp)_4]^{2+}$ unit and the anions and the cation resides on a general position in $P\bar{1}$. Only minor disorder in one methylenic carbon atom in one of its hpp ligands is observed. Because of the high degree of disorder in **5** and its close chemical similarity to **6**, only the $[W_2(hpp)_4]^{2+}$dication in **6** is presented in Figure 1.

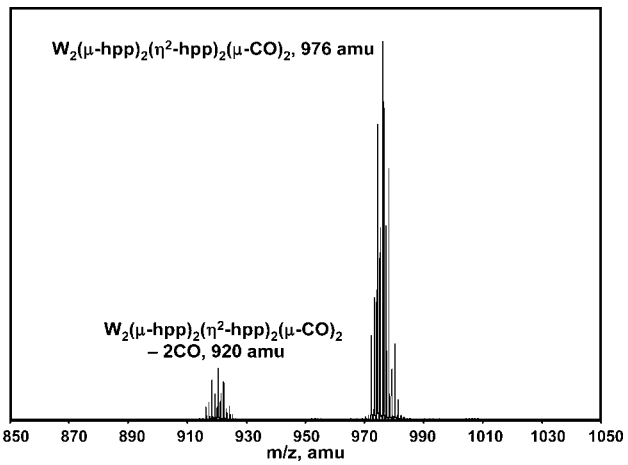

Figure 2. ESI$^+$ mass spectrum of **2**. The signal centered at 920 amu is consistent with the loss of both μ-CO ligands and formation of $W_2(hpp)_4$.

The set of compounds $W_2(hpp)_4Cl_2$, $W_2(hpp)_4(PF_6)_2$, and $[W_2(hpp)_4](TBPF)_2$ comprise a series in which axial ligation to the ditungsten unit varies from the modest interaction of remote Cl^- (2.95[6]/3.064(9)[7] Å) to the weak interaction of PF_6^- (the closest W···F contact is 2.774(5) Å), to the lack of covalent interaction of $TBPF^-$. In the same order, the tungsten−tungsten bond lengths vary from 2.2497(8)[13]/2.250(2)[7] Å (for two independent crystal structures), to 2.2083(7) and 2.1920(3) Å. Considering the small esd's on these bond distances, these changes are significant and this range is surprisingly large for metal−metal bonded compounds in the same oxidation state with the same set of bridging ligands and suggests that even weak axial interactions in these dimetal complexes have an effect upon the metal−metal bond length greater than what has been previously recognized.[53] Calculations at the DFT level, to be presented later,

(52) It should be remembered that $W_2(hpp)_4$ will be instantaneously oxidized to $W_2(hpp)_4Cl_2$ even at ambient temperature by chlorinated solvents such as CH_2Cl_2. See ref 6.

(53) Another factor that may affect the W−W distances is the planarity or nonplanarity of the CN_3 unit in the bicyclic guanidinate ligand. A stronger interaction with the electrons in δ orbitals is expected from a planar unit than a nonplanar unit. However, it appears that, despite the disorder observed in the hpp units, the CN_3 units are nearly planar in all three compounds.

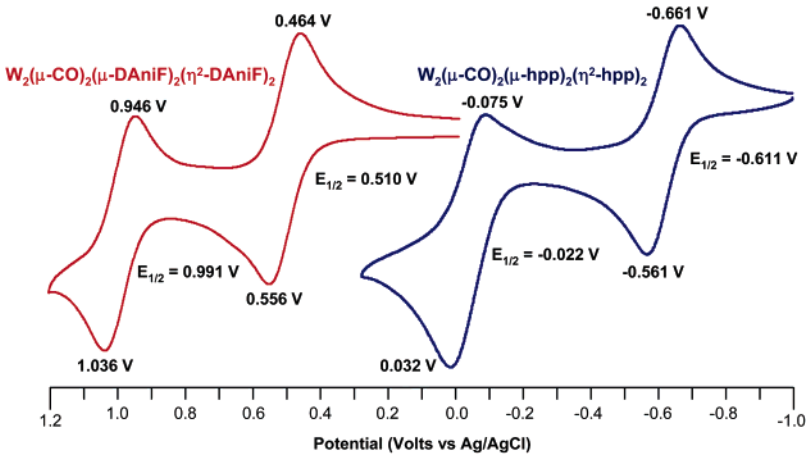

Figure 3. CV of **2** in CH_2Cl_2 (right) and that of the formamidinate analogue $W_2(\mu\text{-}CO)_2(\mu\text{-}DAniF)_2(\eta^2\text{-}DAniF)_2$ (left) which was prepared according to ref 18. Note the greater stabilization of the oxidized species of the guanidinate derivative relative to that with formamidinate ligands.

provide information as to why such variations in metal−metal distances are present in these three compounds.

Electrochemistry. Cyclic voltammetry in CH_2Cl_2 upon **2** and $W_2(\mu\text{-}CO)_2(\mu\text{-}DAniF)_2(\eta^2\text{-}DAniF)_2$ (Figure 3) reveals the dramatically stronger destabilization of the dimetal MOs and the greater electron-donating capacity of the hpp ligand as compared to the DAniF ligand. Compound **2** undergoes a very facile and reversible one-electron oxidation at −0.611 V vs Ag/AgCl and a second quasi-reversible oxidation at −0.022 V. The quasi-reversible nature of this second wave may be due to loss of CO, which is consistent with the $W_2(hpp)_4$ peak noted in the ESI^+ mass spectrum of this compound and subsequent reaction with CH_2Cl_2. In contrast to **2**, the first oxidation for $W_2(\mu\text{-}CO)_2(\mu\text{-}DAniF)_2(\eta^2\text{-}DAniF)_2$ occurs at 0.510 V under the same conditions,[18] a shift of 1.12 V in the oxidizing direction for the same process in a nominally similar compound. A second, reversible oxidation in $W_2(\mu\text{-}CO)_2(\mu\text{-}DAniF)_2(\eta^2\text{-}DAniF)_2$ occurs at 0.991 V.[18] The tremendous electron richness of the hpp ligand has been recognized for some time and has been usefully applied in the preparation of dimetal compounds, such as $[Os_2(hpp)_4Cl_2]PF_6$[54] and $[Re_2(hpp)_4Cl_2]PF_6$,[55] which possess core oxidation states that are too high to be sufficiently stabilized by other ligand systems, including formamidinates. To our knowledge, however, **2** and $W_2(\mu\text{-}CO)_2(\mu\text{-}DAniF)_2(\eta^2\text{-}DAniF)_2$ represent the first pair of isostructural, isoelectronic dimetal compounds in which the difference between the electron-donating capabilities of hpp and a commonly used formamidinate have been compared and quantified by electrochemical measurements.

Due to its poor solubility, no electrochemical measurements have been carried out on **4**. However, the fact that the products of two chemical reductions exist, namely $W_2(hpp)_4Cl$ and $W_2(hpp)_4$, implies that two reversible reduction processes occur in this system. Changing the Cl^- counteranions in **4** to PF_6^- in **5** and $TBPF^-$ in **6** increased the solubility of the $W_2(hpp)_4^{2+}$ core and allowed the study of its electrochemical behavior. Differential pulse voltammetry upon **6** in THF shows two peaks at −0.94 and −1.78 V, which represent a reduction process with $E_{1/2}$ of −0.97 for the first and −1.81 V for the second. These are the most negative potentials recorded for any dimetal bonded species, a fact which is reasonable since the fully reduced species $W_2(hpp)_4$ is the most easily ionized molecule in the gas phase recorded to date. These electrode potentials are indicative that $W_2(hpp)_4$ is a strong reducing agent. Early exploratory work has shown that $W_2(hpp)_4$ easily reduces TCNQ (TCNQ = 7,7,8,8-tetracyanoquinonedimethane), C_{60}, and halogenated species such as CH_2Cl_2.[6] It should be noted that the synthetic chemist has rather few choices for strong chemical reducing agents that are soluble in organic solvents.[56] Thus, it is expected that $W_2(hpp)_4$ will now join the group of well-known reducing agents, e.g., Cp^*_2Co and Cp^*_2Cr, the latter of which is competent even at reducing coordinated dinitrogen.[57] A possible advantage of the unsaturated hpp ligands is that these species are less likely to be susceptible to secondary reactions such as deprotonations and nucleophilic attacks observed occasionally on the π systems of the rings such as Cp_2Co^+ or $Cp^*_2Co^+$.[58]

Photoelectron Spectroscopy. The gas-phase valence PES of $W_2(hpp)_4$ in the energy range from 3 to 10 eV is compared to the previously reported spectra of $W_2(OAc)_4$ (OAc = acetate)[59] and $W_2(DPhF)_4$ (DPhF = *N*,*N*′-diphenylformamidinate)[60] in Figure 4. The spectrum of $W_2(OAc)_4$ shows ionizations from the metal−metal σ (8.54 eV), π (7.84 eV), and δ (6.07 eV) orbitals. Ionizations from the acetate ligands are at higher energy and are not seen in this region of the spectrum. The PES of $W_2(DPhF)_4$, shown in the middle of

(54) Cotton, F. A.; Dalal, N. S.; Huang, P.; Murillo, C. A.; Stowe, A. C.; Wang, X. *Inorg. Chem.* **2003**, *42*, 670.
(55) Berry, J. F.; Cotton, F. A.; Huang, P.; Murillo, C. A. *Dalton Trans.* **2003**, 1218.
(56) (a) Connelly, N. G.; Geiger, W. E. *Chem. Rev.* **1996**, *96*, 877. (b) Ruiz, J.; Astruc, D. *C. R. Acad. Sci., Ser. IIc: Chim.* **1998**, *1*, 21.
(57) (a) Yandulov, D. V.; Schrock, R. R. *Science* **2003**, *301*, 76. (b) Schrock, R. R. *Chem. Commun.* **2003**, 2389.
(58) See for example: Wildschek, M.; Rieker, C.; Jaitner, P.; Schottenberger; H.; Schwarzhans, K. E. *J. Organomet. Chem.* **1990**, *396*, 355.
(59) (a) Lichtenberger, D. L.; Kristofzski, J. G. *J. Am. Chem. Soc.* **1987**, *109*, 3458. (b) Chisholm, M. H.; Clark, D. L.; Huffman, J. C.; Van Der Sluys, W. G.; Kober, E. M.; Lichtenberger, D. L.; Bursten, B. E. *J. Am. Chem. Soc.* **1987**, *109*, 6796.
(60) Lichtenberger, D. L.; Lynn, M. A.; Chisholm, M. H. *J. Am. Chem. Soc.* **1999**, *121*, 12167.

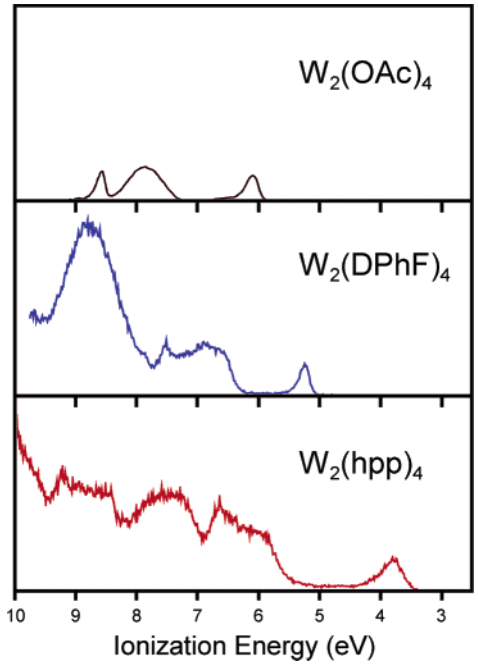

Figure 4. The large effect of the ligand on the δ ionization (last peak on the right) for the quadruply bonded W_2^{4+} species, $W_2(O_2CCH_3)_4$ (top, ref 59), $W_2(DPhF)_4$ (center, ref 60), and $W_2(hpp)_4$ (bottom).

Figure 4, has been discussed in detail[60] and assigned using information from ionization intensity changes with He I, He II, and Ne I excitation and energy shifts in the Cr, Mo, and W series. The δ ionization of $W_2(DPhF)_4$ at 5.23 eV is again the first ionization and is destabilized 0.84 eV from that of $W_2(OAc)_4$. This ionization is followed by ligand-based ionizations between 6 and 7 eV that are associated with orbitals that are primarily nitrogen lone pair in character and by the metal−metal σ and π ionizations located around 7.5 eV. The intense ionization band from 8 to 9 eV is mostly due to ionizations of phenyl π orbitals; there are also additional nitrogen-based ligand ionizations in this energy region.

The spectrum of $W_2(hpp)_4$ shown in Figure 4 is of much higher quality, particularly much better signal-to-noise, than the spectrum of only 3.2−4.5 eV that we reported previously.[1] The vertical ionization energy and onset of the δ ionization of $W_2(hpp)_4$ agrees with our previously reported values of 3.76 ± 0.02 eV for the vertical energy and 3.51 ± 0.05 eV for the onset energy. Previous to the discovery of this molecule, the lowest reported ionization energy for a closed-shell molecule that could be prepared in gram quantities was 4.87 eV for $W(dmpe)_3$ (dmpe = 1,2-bis-dimethylphosphinoethane).[61] The δ ionization of $W_2(hpp)_4$ is destabilized 1.47 eV from that of $W_2(DPhF)_4$. This is followed at higher energy by ionizations that are for the most part associated with the hpp ligands, with the metal−metal σ and π ionizations not clearly visible. Further spectroscopic studies are currently ongoing to aid in the definitive assignment of the other metal−metal ionizations of $W_2(hpp)_4$, as well as those of its Cr and Mo congeners.

(61) Jatcko, M. E., Ph.D. Dissertation, The University of Arizona: Tucson, AZ, 1989.

Table 6. Bond Parameters and Energies from DFT Calculations

	calculated bond distances (Å)		
compound	W−W	W−Cl	W−N
$W_2(hpp)_4Cl_2$	2.2735	2.9620	2.1196
$Cl\cdots W_2(hpp)_4\cdots Cl$	2.2086	14.0[a]	2.1080
$[W_2(hpp)_4]^{2+}$	2.1990	−	2.0971

[a] Distance fixed in the calculation.

DFT Calculations and Electronic Structures. Compounds **4**, **5**, and **6** show different levels of axial interactions and significant variations in their W−W bond distances. It is unusual that, while **4** shows *very long* W−Cl separations (3.064(9)),[7] which are not usually expected to influence other bonding distances, its effect on the W−W bond appears to be significant when compared to **5** and **6**. These compounds have weak axial donor and no axial interaction, respectively, but considerably shorter W−W bond distances. The electronic structure of **4** and the axial interactions of the Cl^- ligands have been examined by the Chisholm group using DFT calculations, which reproduced accurately its geometry.[13] From an analysis of the figures provided in that work, it is apparent that long-range interactions exist between the Cl p orbitals and both the σ and the π metal-based orbitals. It is also apparent that the metal-based σ and π interactions are perturbed by the pσ and pπ orbitals of the Cl^- ions. The filled σ orbital interacts with the symmetric combination of the filled pσ orbitals (hereafter abbreviated as 2Clpσ_s) of the chloride anions to generate two molecular orbitals, one bonding (σ+2Clpσ_s) and one antibonding (σ−2Clpσ_s) between the W_2 unit and the chloride anions. In fact, the antibonding member of this set, σ−2Clpσ_s, is the HOMO. The metal−metal π orbitals are also disturbed in a similar way by the axial ligand, although to a lesser extent.

We have performed a comparative analysis on two models of **4** with different W−Cl distances to better establish the destabilization effect of the axial Cl^- ions and to compare them with the values experimentally found in our structural study of $W_2(hpp)_4^{2+}$ species without axial ligands. The first model consists of the optimized geometry of **4**, under no constraints nor simplifications, and by having the crystal structure parameters as the starting geometry, which is similar to the calculation reported by Chisholm.[13] In the second model, the two W−Cl distances were constrained to a fixed value of 14.0 Å and the rest of the molecule was permitted to relax to its optimum geometry. At these long axial distances, no W···Cl overlap is expected, and this model resembles compound **6**. Selected calculated bond distances are shown in Table 6. The model with shorter W−Cl distances reproduces quite well the crystal structure of **4**. It predicts a long W−Cl distance (2.9620 Å), and a long W−W bond (2.2735 Å). In contrast, a shortening of the W−W bond, by as much as 0.06 Å, is the main structural effect of pulling the axial Cl ligands away from the metal atoms in the second model. This implies that the Cl^- ions have a destabilizing effect on the bonding between the W atoms and is consistent with what is observed experimentally among compounds **4**, **5**, and **6**.

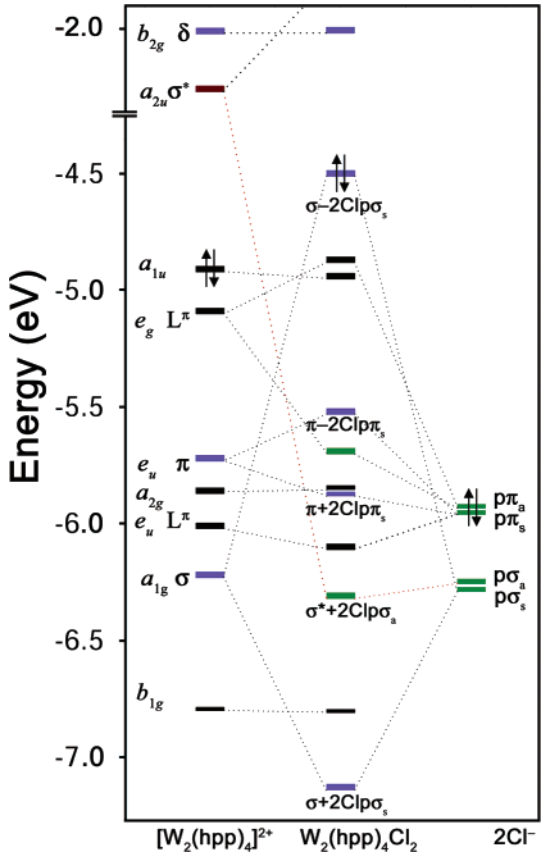

Figure 5. MO diagram for the unrestrained model of **4** with W−Cl distances (2.96 Å). The 'a' and 's' subscripts refer to the antisymmetric and symmetric combinations of the Cl p orbitals with respect to the mirror plane that bisects the molecule between the two W atoms.

The calculated Mulliken overlap population between the W atoms in the model with elongated Cl distances, 0.76, is much larger than the overlap for the model with short Cl distances, 0.36. To understand the origin of this increase in the W−W overlap population with increase in W−Cl distance, as well as the concomitant decrease in the W−W bond distance, a fragment analysis was performed on both $W_2(hpp)_4Cl_2$ models. Figure 5 show the MO diagram, constructed by the fragments of $[W_2(hpp)_4]^{2+}$ and $2Cl^-$ ions, at the unrestrained W−Cl distances. On the left of the diagram are the MOs of the $[W_2(hpp)_4]^{2+}$ dication, and the metal-based orbitals are shown in blue. On the right of Figure 5 is the set of six occupied MOs contributed by the occupied p orbitals of both Cl^- ions, and in the center are the MOs of the $W_2(hpp)_4Cl_2$ molecule, where the W and Cl p orbital interactions can be clearly seen. The importance of this fragment analysis is that it shows that the σ^* virtual orbital of the $[W_2(hpp)_4]^{2+}$ fragment interacts with the filled antisymmetric combination of the Cl pσ orbitals and gains a large Mulliken occupation of 0.249 in the $W_2(hpp)_4Cl_2$ molecule. This indicates that, even at long W−Cl distances, 2.96 Å, the Cl^- ions donate about 1/4 of a charge into the antibonding virtual σ^* orbital,[62] which in turn causes an

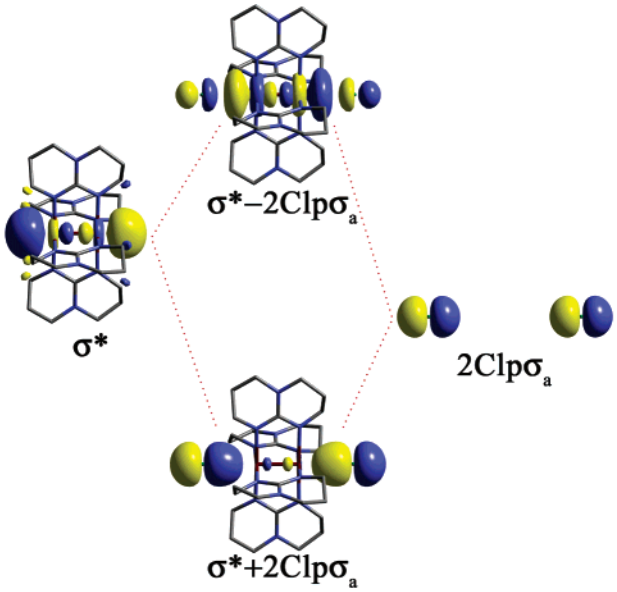

Figure 6. The 0.03 surface contour diagrams of the σ^* and $2Clp\sigma_a$ interactions. Note the antibonding σ^* character between the W atoms in the $\sigma^*+2Clp\sigma_a$ orbital.

increase in the W−W bond distance. The mechanism of this charge donation has its origin in a small, but symmetry allowed, interaction between the antisymmetric combination of the filled σp orbitals of the chloride anions ($2Clp\sigma_a$), and the empty σ^* orbital of the metal atoms to form $\sigma^*+2Clp\sigma_a$. This interaction contributes bonding character between the W_2 unit and the chloride anions but introduces antibonding character between the two metal atoms,[63,64] as shown in red in Figure 5 and depicted graphically in Figure 6.

The MOs of the $[W_2(hpp)_4]^{2+}$ dication are illustrated in Figure S1. The four highest occupied orbitals are ligand-based. The HOMO-4 is the first metal-based orbital and is a π orbital. The σ orbital lies still further down in energy as the HOMO-6. This is the electronic structure anticipated for the removal of two electrons from the quadruply bonded $W_2(hpp)_4$ molecule.

It is evident that by increasing the W−Cl distance, which removes the axial interactions, the charge donation into the σ^* orbital should be eliminated. Indeed, the fragment analysis on the model with long W−Cl distances shows that the Mulliken population of the σ^* orbital of the $[W_2(hpp)_4]^{2+}$ cation is zero, and thus, it predicts a shorter W−W bond

(62) This σ^* orbital has a W contribution of 93% and is composed of the antisymmetric combinations of the $5d_{z^2}$, $6p_z$, and 6s orbitals that contribute 34%, 50%, and 9%, respectively, as obtained from this calculation.

(63) This situation is analogous to that in transition metal carbonyls in which back-bonding contributes to M−C bonding but the interaction is antibonding with respect to C−O bonding. If carbonyl ligands are regarded as σ donors and π^* acceptors, the $[W_2(hpp)_4]^{2+}$ unit may be viewed as a σ^* acceptor.

(64) Another possible factor influencing the observed differences in W−W bond distances in **4**, **5**, and **6** is the trans influence of the Cl ligands that weakens the W−W bond. (See: Kiehl, P.; Rohmer, M.-M.; Bénard, M. *Inorg. Chem.* **2004**, *43*, 3151.) This rationalization has been used to explain changes in metal−metal distances of trinickel chains when axial ligands are removed. It should be noted, however, that calculations by Chisholm et al.[13] have shown that, for the hypothetical molecule $W_2(hpp)_4H_2$, the W−W bond distances also decrease relative to the chloride analogue. Since H^- is generally considered to have a stronger trans influence than Cl^-, one would expect the calculated W−W distances to increase even more for this compound. The fact that this does not occur indicates that Bénard's suggestion is not applicable to the $W_2(hpp)_4X_2$ system.

distance than for the model with shorter W−Cl distances.[65] Figure S2 shows the MO diagram for the model having long W−Cl distances, and as expected, the $[W_2(hpp)_4]^{2+}$ and $2Cl^-$ fragments no longer interact. Thus, the electronic structure of the $[W_2(hpp)_4]^{2+}$ fragment describes the electronic structure of the dication in **6** and to some extent **5**.

The fragment analysis also provides information as to why the W−Cl bonds in **4** are long. The formal bond between the $[W_2(hpp)_4]^{2+}$ and $2Cl^-$ fragments obtained by donation from the antisymmetric combination of the Cl p orbitals, $2Clp\sigma_a$, to the empty σ^* orbital accounts for a formal half bond for each W−Cl interaction. The symmetric combination of the Cl p orbitals, $2Clp\sigma_s$, cannot donate any electrons to the σ orbital because this orbital is already filled. Thus, it is clear that the two W−Cl interactions cannot be described as typical two-electron bonds, but rather as one-electron dative bonds on average. Consistent with this interpretation, the calculated Mayer bond order[66] for the W−Cl interactions, 0.58, approximates a bond order of 1/2 between the tungsten atoms and the chlorine atoms. Moreover, since the metal σ-to-$2Clp\sigma_s$ interaction occurs between filled orbitals, such interaction is repulsive. These factors are responsible for the long W−Cl bonds.[67]

Finally, a time-dependent DFT calculation on the optimized geometry of the dication $[W_2(hpp)_4]^{2+}$ was performed to determine the nature of the lowest-energy transition of the dications in **5** and **6** (Figures S2 and S3, respectively). The calculations indicate that this rather strong absorption is due to a $\pi \rightarrow \delta$ transition that is permitted only in *xy* polarization (experimentally observed at 360 nm, $\epsilon = 33\,000$ M^{-1} cm^{-1}; calculated at 437 nm, $f = 0.0074$). The energy of this transition is somewhat higher than the $\delta \rightarrow \delta^*$ transitions observed in typical quadruply bonded paddlewheel complexes such as $W_2(DAniF)_4$.

Summary and Conclusions

Reaction of $W(CO)_6$ in chlorobenzene or *o*-dichlorobenzene with the guanidine-type ligand Hhpp can be used to produce $W(Hhpp)_2(CO)_4$ (**1**), $W_2(\mu\text{-}CO)_2(\mu\text{-}hpp)_2(\eta^2\text{-}hpp)_2$ (**2**), or $W_2(hpp)_4Cl_2$ (**4**) depending upon the particular reaction conditions employed. It is probable that formation of $W_2(hpp)_4Cl_2$ proceeds through the intermediacy of **1** and **2**. These results contrast sharply with those in the analogous system with HDAniF in which $W_2(\mu\text{-}CO)_2(\mu\text{-}DAniF)_2(\eta^2\text{-}DAniF)_2$ was isolated in low yield accompanied by other species that indicate decomposition of the HDAniF ligand. The differences between the product manifolds of these two systems are due to the generally more robust character and the higher thermal stability of the hpp ligand.

Compounds **2** and $W_2(\mu\text{-}CO)_2(\mu\text{-}DAniF)_2(\eta^2\text{-}DAniF)_2$ constitute a pair of isostructural, isoelectronic dimetal compounds with the hpp and DAniF ligands that has been thoroughly characterized by electrochemistry and by a variety of spectroscopic methods. Thus, **2** and $W_2(\mu\text{-}CO)_2(\mu\text{-}DAniF)_2(\eta^2\text{-}DAniF)_2$ provide a sharp focus and strong emphasis upon the differences between these two types of nitrogen ligand anions. Consistent with the gas-phase photoelectron spectroscopy results described above, the hpp ligand is found to be emphatically more basic than the DAniF ligand, so much so that **2** is more readily oxidized than $W_2(\mu\text{-}CO)_2(\mu\text{-}DAniF)_2(\eta^2\text{-}DAniF)_2$ by 1.12 V. This effect is also evident when the potentials in CH_2Cl_2 for the W_2^{5+}/W_2^{4+} processes for $W_2(hpp)_4$ and $W_2(DAniF)_4$[18] are compared. These values are −1.156 V[68] for the former and −0.336 V[69] vs Ag/AgCl for the latter, a difference of 0.82 V. The changes in potentials are also consistent with the fact that $W_2(hpp)_4$ is more readily ionized than $W_2(DPhF)_4$ by 1.4 eV.

The DFT-calculated structure for $W_2(\mu\text{-}CO)_2(\mu\text{-}DAniF)_2(\eta^2\text{-}DAniF)_2$ that was reported in earlier work[18] revealed that a strong W → CO π^* back-bonding interaction was the basis for the pronounced $D_{2h} \rightarrow C_{2h}$ symmetry distortion in this compound and the HOMO had both tungsten−tungsten bonding and W → CO π^* back-bonding character. The same qualitative MO description applies to **2**, but the W → CO π^* back-bonding interaction is significantly enhanced due to the greater electron density added by the hpp ligand anions to the W_2^{4+} core. This description of **2** is confirmed by isolation and characterization of the PF_6^- salt of $[W_2(\mu\text{-}CO)_2(\mu\text{-}hpp)_2(\eta^2\text{-}hpp)_2]^+$ (**3**), the one-electron oxidized homologue of **2**. The structural and IR spectroscopic changes observed in oxidizing **2** to **3** support the foregoing description of the nature of the HOMO in **2**.

For the $W_2(hpp)_4X_2$ species, X = Cl, PF_6, and TFPB, there are significant variations in the W−W distances. The longest separation is in the compound in which X = Cl. The cause of this lengthening is a donation of electron density by the weakly coordinated Cl^- ions into the W−W σ^* orbital. We anticipate that such an effect will be observable in other paddlewheel species with axial chloride groups and M_2^{n+} cores that have an empty σ^* orbital.

Finally, it is important to note that excellent yields of $W_2(hpp)_4Cl_2$, a key intermediate for the preparation of the most easily oxidized closed-shell molecule, have now been obtained in one step from reaction of the commercially available compounds $W(CO)_6$ and Hhpp at 200 °C in *o*-dichlorobenzene. Because $W_2(hpp)_4$ can be easily prepared in one additional step from $W_2(hpp)_4Cl_2$, further development

(65) Note that the elongation of M−M bonds by Cl axial interactions in paddlewheel compounds should not be limited to the W_2 system. Any bonded M_2 system with Cl axial ligands and an empty σ^* orbital may be expected to experience some degree of elongation of the M−M bond.

(66) Mayer, I. *Chem. Phys. Lett*. **1983**, *97*, 270.

(67) Another apparent explanation as to why the W−Cl distances are so long is because steric hindrance of the H atoms in the hpp ligand. However, we have made an entire series of $M_2(hpp)_4Cl_2$ compounds with M = Mo, W, Ru, Re, Os, Ir, Pd, and Pt. (see Cotton, F. A.; Murillo, C. A.; Wang, X.; Wilkinson, C. C. *Inorg. Chim Acta* **2003**, *351*, 191 and references therein). In those compounds, the M−Cl distances vary from 2.47 to 3.17 Å. The short distance of 2.47 Å (for the Pd compound) seems to indicate that the Cl atoms can approach the metal atoms without problems.

(68) In CH_2Cl_2, the CV of $W_2(hpp)_4Cl_2$ shows only one reversible wave at −1.156 V vs Ag/AgCl for the W_2^{5+}/W_2^{4+} process. This value is shifted toward a more negative potential relative to that in THF (−0.97 V). As expected, the process W_2^{6+}/W_2^{5+} is not observed in CH_2Cl_2.

(69) For the tolyl analogue $W_2(DTolF)_4$, the potential for the W_2^{5+}/W_2^{4+} process has been reported at −0.280 V vs Ag/AgCl in CH_2Cl_2 solutions. See: Cotton, F. A.; Ren, T. *J. Am. Chem. Soc*. **1992**, *114*, 2237.

of $W_2(hpp)_4$ as a clean, powerful inorganic reducing agent is now possible. The fact that $W_2(hpp)_4Cl_2$ can be stored indefinitely using standard Schlenk techniques, as well as that $W_2(hpp)_4$ is thermally stable to at least 300 °C under vacuum, offers great promise for using the $[W_2(hpp)_4]^{n+}$ system as a starting point for further exploratory syntheses. Additionally, the ease with which the rather insoluble $W_2(hpp)_4Cl_2$ is converted to more soluble forms has permitted more complete spectroscopic and electrochemical characterization of this interesting dication.

Acknowledgment. We thank the National Science Foundation, the Robert A. Welch Foundation, and Texas A&M University for funding the research reported here. J.P.D acknowledges the support of an NIH postdoctoral fellowship. We also thank Dr. Chad Wilkinson for providing the sample of K^+TFPB^- used in this study and the TAMU Laboratory for Molecular Simulation for helpful discussions and software.

Supporting Information Available: MO diagram for the model of **4** with restrained W−Cl distances of 14.0 Å (Figure S1), frontier molecular orbitals for the cation of compounds **5** and **6** (Figure S2), electronic spectra of **5** (Figure S3) and **6** (Figure S4), and displacement ellipsoid plots at the 30% probability level with complete atomic labeling for compounds **1**−**3**, **5**, and **6**, (Figures S5−S9), and for the crystal structures described in refs 47, 48, and 51 (Figures S10−S12) in PDF format. X-ray crystallographic data in standard CIF format are also available for these compounds, as well as for the structures cited in refs 47, 48, and 51. This material is available free of charge via the Internet at http://pubs.acs.org.

IC0515709